Optical properties of BN in cubic and layered hexagonal phases

Giancarlo Cappellini and Guido Satta
INFM Sezione di Cagliari and Dipartimento di Fisica, Università di Cagliari, Cittadella Universitaria, Strada Provinciale Monserrato-Sestu Km 0.700, I-09042 Monserrato (Ca), Italy

Maurizia Palummo and Giovanni Onida
INFM Sezione di Roma-2 and Dipartimento di Fisica, Università di Tor Vergata, Via della Ricerca Scientifica 1, I-00133, Rome, Italy
(Received 24 January 2001; revised manuscript received 6 April 2001; published 26 June 2001)

Linear optical functions of cubic and hexagonal BN have been studied within first principles density functional theory in the local density approximation. Calculated energy-loss functions show reasonable agreement with experiments and previous theoretical results both for *h*-BN and for *c*-BN. Discrepancies arise between theoretical results and experiments in the imaginary part of the dielectric function for *c*-BN. Possible explanations of this mismatch are proposed and evaluated: lattice constant variations, *h*-BN contamination in *c*-BN samples, and self-energy effects.

DOI: 10.1103/PhysRevB.64.035104 PACS number(s): 78.20.Ci, 68.35.Ja, 71.45.Gm

I. INTRODUCTION

The properties of boron nitride (BN) have motivated detailed theoretical and experimental studies for a long time.[1–3] Many advanced technologies rely on boron nitride and on materials based on it, due to the wide spectrum of properties offered by its polymorphic modifications, two graphitelike and two dense ones. Boron nitride shares many of its properties, structures, processing and applications with carbon. Cubic boron nitride (also known as sphalerite boron nitride and abbreviated as *Z*-BN, *c*-BN, or β-BN), with sp^3-hybridized B-N bonds, has the diamond crystal structure and a similar lattice constant. Its physical properties, such as extreme hardness, wide energy band gap, low dielectric constant, and high thermal conductivity, are also very near to those of diamond. These unusual properties of *c*-BN have many appealing applications in modern microeletronic devices, and make it useful also as a protective coating material or in heavy-duty tools.[4] Hexagonal BN (*h*-BN or α-BN), an sp^2-bonded layered compound, and graphite also resemble each other in terms of crystal structure, lattice constant, and physical properties such as strong anisotropy. Due to its high thermal stability *h*-BN is a widely used material in vacuum technology. It has been employed in microelectronic devices,[5] for x-ray lithography masks,[6] and as a wear-resistant lubrificant.[7] The hexagonal phase is also the underlying structure of BN nanotubes, which are systems of growing interest at present.[8–10]

On the other hand, significant differences exist between carbon and boron nitride, due mainly to differences in their chemical bonding. In fact *h*-BN and *c*-BN mechanical strengths, thermal conductivities, and Debye temperatures are lower than in their carbon counterparts. Moreover, *h*-BN is electrically an insulator, while graphite is a conductive semimetal. In contrast to diamond, which can be readily doped only as a *p*-type material, *c*-BN can be doped either *n* or *p* type. Moreover, *c*-BN does not react with ferrous materials, even at high temperatures ($T \sim 1600$ K),[11] and, last but not least, both *c*- and *h*-BN are more resistant to oxidation than their carbon counterparts.[4]

An important issue is the experimental evidence for negative electron affinity (NEA) in cubic boron nitride samples.[12,13] The electron affinity of a semiconductor is the difference between the vacuum energy level and the conduction band minimum level. NEA occurs when the conduction band minimum lies above the vacuum energy level. Any electron promoted into the conduction band then has enough energy to escape into vacuum. One of the most striking applications is in electron emission devices, to obtain the highest electron emission density with the least energy expenditure (cold cathode emitters).[14] Correct evaluation of the one-electron transition energies and the position of the single-particle states turn out to be fundamental points relative to this issue, and will be addressed here in detail.

It is now generally agreed experimentally that bulk *c*-BN is the thermodynamically stable phase in ambient conditions, and that the less dense *h*-BN becomes stable at temperatures exceeding $T \sim 1200$ K.[15] Due to the large change in volume, fragmentation and disordering between the two phases can develop. In combination with a rigid lattice, this leads to a large hysteresis of phase transitions. This means that phases created under high-pressure high-temperature conditions can persist inside the sample under standard conditions.[15] Two other phases, rhombohedral (*r*-BN) and wurtzite (*w*-BN), are stable only at very high pressure ($P \simeq 10$ GPa),[16] and will not be considered here. Structural and excitation properties of the wurtzite structure have been reported elsewhere.[17] At ambient pressures an interplay between *h*-BN and *c*-BN domains only should be expected.[18,19] Since 1979 *c*-BN chemical vapor deposited films have been realized,[20] but the production of pure *c*-BN thin films (by either chemical or physical vapor deposition) remains a difficult task due to the formation, during the growth process, of unwanted *h*-BN domains.[19]

Extensive theoretical studies have been performed on the ground-state properties of BN. All calculations founded on density functional theory (DFT) and on the local density approximation (LDA) for the exchange-correlation potential agree in predicting that the *c*-BN structure has a lower energy than *h*-BN by about 0.06 eV per atom.[21–24] This result,

which is confirmed by our calculation, disagrees with an older calculation based on the orthogonal linear combination of atomic orbitals (OLCAO), where *h*-BN was found to be more stable than *c*-BN by 0.35 eV per atom.[25] This is probably explained by a lack of convergence in the older calculations. The band structure properties of BN have also been the subject of extensive theoretical work, performed within different schemes and approximations.[1,2,8–10,21–25,17,26–37] From the experimental point of view many methods have been employed to explore the electronic structure. Among them there are methods like soft-x-ray emission spectroscopy[38,39] and photoelectron spectroscopy,[40] which are both sensitive to occupied states, as well as near-edge x-ray absorption fine structure spectroscopy[41,42] and energy-loss near-edge spectroscopy, which can be used to probe the empty bands.[43] In addition, electron energy-loss spectroscopy performed in the plasmon region has proved to provide valuable information.[43–45]

The experimental optical functions of BN compounds are not as well known as those of the other group III nitrides. This is due in large part to the lack of high-quality single-crystal samples. Consequently, most optical studies on BN have been performed on polycrystalline samples, with various amounts of impurities. As one would expect, the results of optical studies performed on these materials vary greatly.[46,47] However, a general consensus from the experimental data is that the minimum band gap is direct in the case of *h*-BN and indirect in the case of *c*-BN. For *h*-BN a direct band gap of 5.2 ± 0.2 eV associated with the transition H_{3v}-H_{2c} has been estimated,[48] while a value of 6.4 ± 0.5 eV for the indirect minimum band gap in *c*-BN has been determined,[49] and associated with the Γ_{15v}-X_{1c} transition.[17,33]

In the present paper we present *ab initio* linear optical functions of *c*- and *h*-BN studied within DFT-LDA. No external parameter has been used to fit the experimental curves. Due to the importance of the two BN phases and to the fact that in several experimental configurations they appear together in the same sample, a parallel study of both phases has been accomplished throughout the present paper. Complex dielectric functions, refractive indices, reflectance spectra, optical conductivity, and energy-loss functions for *c*-BN and *h*-BN have been calculated. We report our results in the energy range of interest and compare them with the existing theoretical and experimental literature. Calculated DFT-LDA energy-loss functions agree relatively well with experiments and with previous theoretical results, for both *h*-BN and *c*-BN. On the other hand, discrepancies arise between theoretical results and experiments in the imaginary part of the dielectric function for *c*-BN. Possible explanations of this issue are proposed and evaluated in detail. The imaginary part of the dielectric function in the *h*-BN case, instead, shows a reasonable agreement with both other theoretical results and experiments.

This paper is organized as follows. In Sec. II we give the computational details of the calculation of the ground-state properties for both phases. In Sec. III we describe the theoretical scheme used to evaluate the optical properties, and the part related to the calculation of excitation properties. In Secs. IV and V we present results for the optical properties of *c*-BN and *h*-BN, respectively. Finally, in Sec. VI conclusions are drawn, and the perspectives and issues opened by our work are presented.

II. COMPUTATIONAL DETAILS AND GROUND-STATE CALCULATIONS

Density functional calculations have been carried out within the local density approximation for the exchange and correlation functional,[50] using the Perdew and Zunger parametrization[51] of the Ceperley and Alder results.[52] Kohn-Sham orbitals are expanded in a plane-wave basis set, with an energy cutoff of 55 Ry.

Care has been used in constructing the ionic pseudopotentials, in order to avoid the occurrence of ghost states and to assure optimal transferrability.[53,54] Angular components up to $l=2$ have been included. Separable, norm-conserving soft pseudopotentials have been generated within the scheme of Troullier and Martins,[55] with the core radii (bohr) 1.59 (B, $3d$) and 1.49 (N, $2p$). For boron, nonlinear core corrections to be used in the solid calculation have been taken into account in generating pseudopotentials and pseudo-wave-functions.[56]

With the selected plane-wave cutoff, both the total energy and Kohn-Sham eigenvalues are converged to better than 0.1 eV for both *c*-BN and *h*-BN. For the cubic phase, the use of 10 special Chadi and Cohen *k* points for charge integration in the first Brillouin zone (BZ)[57] is found to be sufficient to achieve a good accuracy for the computed total energy; for instance, the total energy changes by less than 10 meV and the fundamental band gap by less than 0.1 eV when passing from six to 10 special points for BZ sampling. For the layered haxagonal case the use of 12 *k* points is sufficient for a full convergence of the total energy and eigenvalues.

Hexagonal BN turns out to be less stable than cubic BN by about 0.050 eV/atom. Preliminary calculations in which ''hard'' norm-conserving pseudopotentials of the Bachelet-Hamann-Schlüter (BHS) form were used with energy cutoff[17] of 150 Ry gave an energy difference of 0.078 eV/atom. Our results hence confirm the previous finding that *c*-BN is more stable than *h*-BN. No contributions to the total energy coming from zero point vibrations of the lattices have been considered.[19,21]

In Table I the structural parameters for the two phases are reported, in comparison with previous theoretical calculations and experiments. For *c*-BN our equilibrium lattice parameter underestimates the experimental one by a few percent as usual for DFT-LDA, in accordance with previous theoretical results. The bulk modulus falls very near to the experimental energy range.[21,25]

An underestimation of the same order was found for the two lattice parameters a and c/a of *h*-BN, as reported by other authors also.[21,25]

No large differences in equilibrium structural parameters arise when the harder BHS pseudopotentials and the larger cutoff are used.[17]

TABLE I. Calculated structural properties of zinc-blende and hexagonal BN (lattice constant and bulk modulus) compared with other theoretical and experimental results.

	Present	Ref. 17	Ref. 21	Ref. 25	Expt. (Ref. 17)
			c-BN		
a_0 (a.u.)	6.754	6.771	6.759	6.833	6.833
B_0 (Mbar)	4.01	3.52	3.97	3.70	3.69-4.65
			$h=BN$		
a_0 (a.u.)	4.698	4.68	4.50	4.71	4.72
c/a	2.608	2.6068	2.608	2.670	2.664
B_0 (Mbar)	2.68	2.65	2.61	3.35	

III. OPTICAL PROPERTIES AND ELECTRONIC EXCITATIONS

The experimental scenario for the electronic properties of boron nitride is characterized by many measurements. For *h*-BN, however, old optical and energy-loss data are very conflicting with each other mostly because of the use of poor samples. Band structures calculated in the past were not accurate enough to be of real help.[25] Recently, careful measurements of inelastic electron scattering spectra on well characterized *h*-BN became available,[45] and accurate measurements of the linear optical properties of *c*-BN have been reported.[46] Ellipsometry measurements have also been done to characterize noncrystalline thin films of BN,[45,58] and optical reflectance spectra of *c*-BN have recently been published.[47]

We determine the optical properties of *h*-BN and *c*-BN by calculating the momentum matrix elements associated with dipole transitions at a large number of *k* points in the BZ. The frequency-dependent imaginary part of the dielectric function is given by[59,60]

$$\epsilon''_{\alpha\alpha}(\omega)=\frac{(8\pi)^2e^2}{\omega^2m^2V}\sum_{v,c}\sum_{\vec{k}}|\langle v,\vec{k}|p_\alpha|c,\vec{k}\rangle|^2 \times\delta(E_c(\vec{k})-E_v(\vec{k})-\hbar\omega), \quad (1)$$

where v and c label the valence and conduction states associated with the energies $E_v(\vec{k})$, $E_c(\vec{k})$, V is the crystal volume, and $\langle\rangle$ is the matrix element of the momentum operator. Nonlocality effects in the ionic pseudopotentials are neglected in the evaluation of ϵ_2.[59] Eigenvalues and eigenfunctions appearing in Eq. (1) are those determined within the DFT-LDA scheme. As it appears from Eq. (1), local field effects are also neglected in the dielectric function calculation.[59] For formulas relative to the macroscopic optical functions here calculated we refer to Ref. 61.

To give an overview of the optical properties of the two crystals, and in particular of the differences between the hexagonal and cubic phases, the calculated interband optical conductivity σ is reported in Fig. 1 and in Fig. 2. In the case of *h*-BN, an average over the three crystallographic directions is taken. Both the absorption threshold and the oscillator strengths in *h*-BN are much smaller than in *c*-BN. In the two cases, our data reproduce fairly well the orthogonalized LCAO results of Xu and Ching.[25] Many structures can be directly related to measured ones, like the peak around 6 eV for *h*-BN, which can be assigned to transitions between bands in the in-plane direction. This correspondence reflects the strong anisotropy in the optical absorption of this material, which shows up even when macroscopic quantities are taken into account.

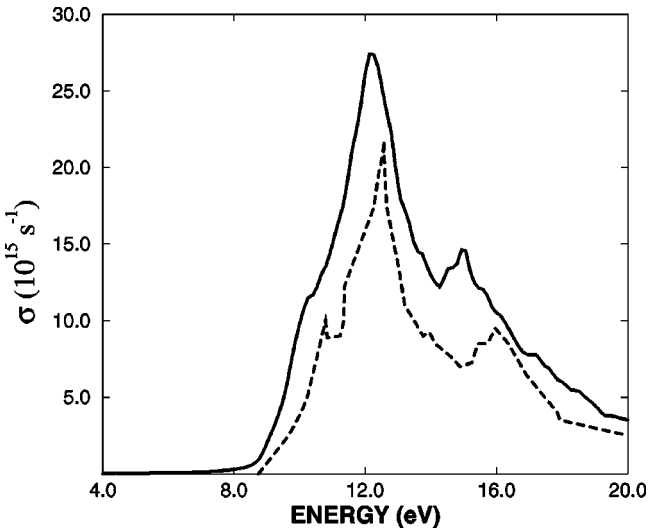

FIG. 1. Calculated optical conductivity σ of *c*-BN (solid line) vs the theoretical result of Ref. 25 (dashed line).

As is well known DFT-LDA band structures for semiconductors and insulators cannot reproduce the real (experimental) ones. DFT-LDA eigenvalues, when interpreted as quasiparticle (QP) energies show the so called band gap problem.[62] The QP energies correspond only qualitatively to the DFT-LDA ones, mainly because the band gaps between conduction and valence bands show a systematic underestimation with respect to the experiments.[63–65] This problem can be solved, for semicon-

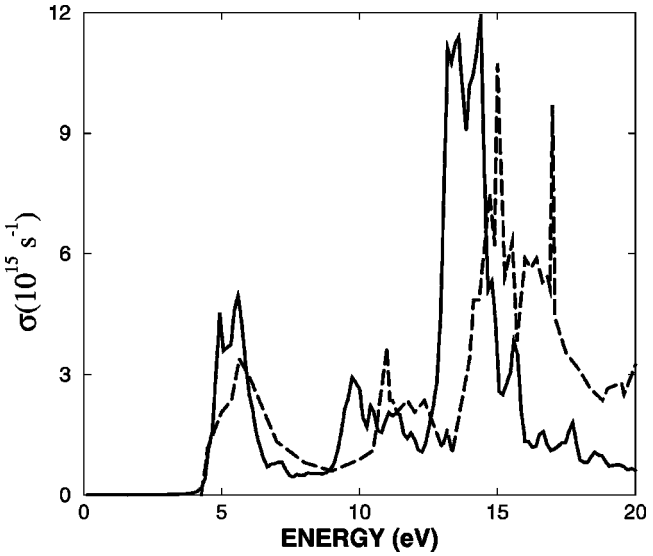

FIG. 2. Optical conductivity function of *h*-BN (solid line) vs previous theoretical result (dashed line) after Ref. 25.

TABLE II. Excitation energies for *c*-BN.

	Present	Ref. 17	Ref. 33	Expt.
$\Gamma_{15'v}$-X_{1c}	7.28	6.95	6.3	6.4±0.5 [a]
$\Gamma_{15'v}$-Γ_{1c}	11.79	11.46	11.4	14.5 [b]

[a]Reference 49.
[b]Reference 3.

ductors and insulators, within a self-energy scheme, called *GW*.[66] Within this method, the self-energy operator reads $\Sigma = GW$, where G is the one-electron Green function and W the screened Coulomb interaction in the system, fully taking into account the screening properties of the material.[62,66,67] The corresponding Dyson equation can be solved within first-order perturbation theory with respect to $(\Sigma - V_{\rm xc})$, where $V_{\rm xc}$ is the DFT-LDA exchange and correlation potential. Assuming the DFT-LDA eigenvalues and eigenfunctions as the zeroth order eigenvalues and eigenfunctions of the system respectively, the QP corrections for the Bloch $\psi_{n\vec{k}}$ state read[62]

$$E_{n\vec{k}} - E^{(0)}_{n\vec{k}} = \frac{\Sigma^{\rm coh}_{n\vec{k}}(E^{(0)}_{n\vec{k}}) + \Sigma^{\rm sex}_{n\vec{k}}(E^{(0)}_{n\vec{k}}) - \langle \psi_{n\vec{k}} | V_{\rm xc} | \psi_{n\vec{k}} \rangle}{1 + d\Sigma_{n\vec{k}}(E)/dE|_{E^{(0)}_{n\vec{k}}}}, \tag{2}$$

where $\Sigma^{\rm coh}_{n\vec{k}}$, $\Sigma^{\rm sex}_{n\vec{k}}$, and $V^{\rm LDA}_{{\rm xc},n\vec{k}}$ are the expectation values of the Coulomb hole (coh) and screened exchange (sex) contributions to the self-energy, and of the DFT-LDA exchange-correlation (xc) potential, respectively.[62] *Ab initio GW* schemes are based on the full calculation of the screening function of the system (i.e., fully including local field and dynamical effects) starting from DFT-LDA eigenvalues and eigenfunctions. These kinds of calculations for semiconductors and insulators have often led to a very good agreement between theory and experiment.[62,67]

Self-energy corrections to the DFT-LDA band structure for semiconductors and insulators can also be performed, with very good results, using a model dielectric function to mimic the real screening of the system.[63–65] One can start from a perturbative formula of the form[68]

$$E_{n\vec{k}} - E^{(0)}_{n\vec{k}} = \frac{\Sigma^{\rm coh}_{n\vec{k}} + \Sigma^{\rm sex}_{n\vec{k}} + \Sigma^{\rm dyn}_{n\vec{k}}(E^{(0)}_{n\vec{k}}) - \langle \psi_{n\vec{k}} | V_{\rm xc} | \psi_{n\vec{k}} \rangle}{1 + d\Sigma_{n\vec{k}}(E)/dE|_{E^{(0)}_{n\vec{k}}}}, \tag{3}$$

where $\Sigma^{\rm dyn}_{n\vec{k}}(E^{(0)}_{n\vec{k}})$ is the zeroth order term of the energy expansion of the dynamical part of Σ, and only the static parts of the sex and coh self-energy are present.[62,68] Corrections to the DFT-LDA spectra calculated from Eq. (3) with the use of model dielectric functions enabled both us and other authors to obtain very positive results, when compared with experiments and *ab initio GW* values, in several semiconductors and insulators.[69,70] Moreover, the use of model screening functions enables one to perform *GW* calculations in a more efficient way, reducing the computational effort by at least one order of magnitude in CPU time.[68,70] Details concerning the evaluation of the different coefficients appearing in Eq. (3) and how they compare with the *ab initio* calculated values are given elsewhere.[69,71]

TABLE III. Excitation energies for *h*-BN . For the meaning of the ''*a*'' and ''*b*'' marks, see text.

	Present	Ref. 17	Ref. 10	Expt. (Ref. 48)
H_{3v}-M_{1c}	6.39	6.04	5.4[a]	5.2±0.2
H_{3v}-H_{2c}	6.76	6.66	6.33[b]	

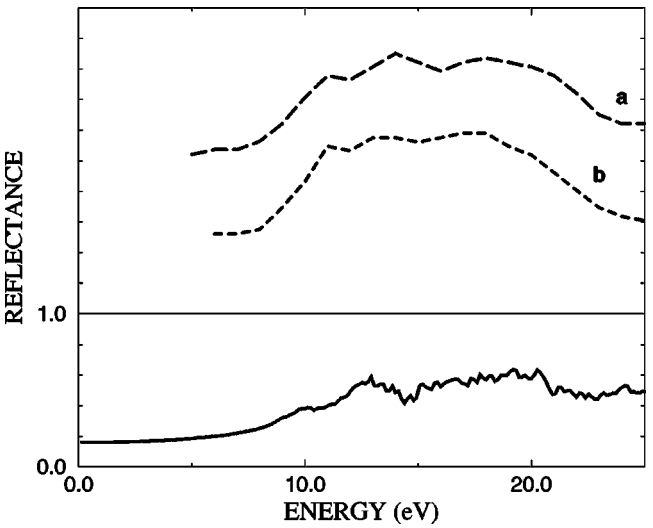

FIG. 3. Calculated reflectance (solid line) of *c*-BN vs experimental results from two samples (see text) in arbitrary units (dashed lines), taken from Ref. 47.

Either *ab initio* or simplified *GW* schemes have been employed to calculate the QP energies of *h*-BN and *c*-BN.[17,33,37,72] All these theoretical results improve the agreement with experimental data. Typically, LDA transition energies suffer from an underestimation of about 3 eV for the cubic phase and 2 eV for the hexagonal one.[17] In Tables II and III for *c*-BN and *h*-BN, respectively, we report the results of previous calculations and experiments, namely, the fundamental gaps and the main transition energies, in comparison with the present results. In *c*-BN the present transition energies have been calculated at the corresponding theoretical lattice constant while in Ref. 33 (as explicitly stated by the authors) the experimental lattice parameter was used. Moreover, the use of an efficient method in a large gap system induces a slight overestimation of the above energies.[17,71] As is clear from the data, minor differences arise between the *ab initio GW* results and the efficient *GW* ones. In Table III, the value marked ''*a*'' correspond to a transition between a point T_1 (along the Γ-K direction near K, and close in energy to H_v) and M_c. The term marked ''*b*'' is the transition energy between K_{3v} and K_{3c}, which is close in energy to the transition H_{3v}-H_{2c}.[33]

IV. CUBIC BN

In Fig. 3 the calculated reflectivity of *c*-BN is displayed together with the experimental data given in Ref. 47 for a

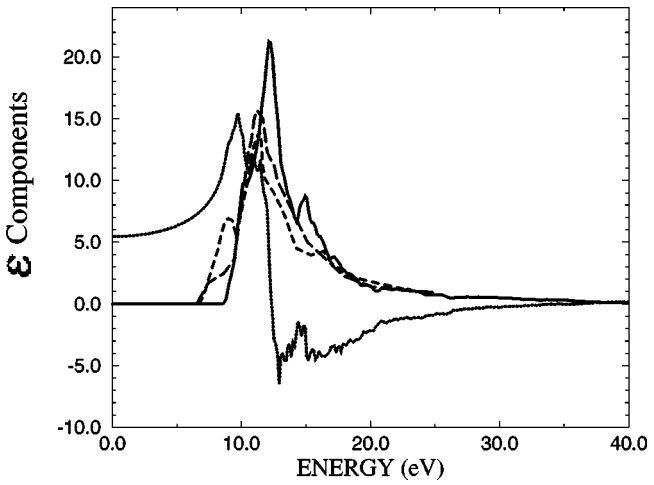

FIG. 4. Calculated imaginary part of dielectric function of *c*-BN (solid line) vs the experimental results of Ref. 47 (dashed lines). Real part of dielectric function computed in the present work (dotted line) is also reported.

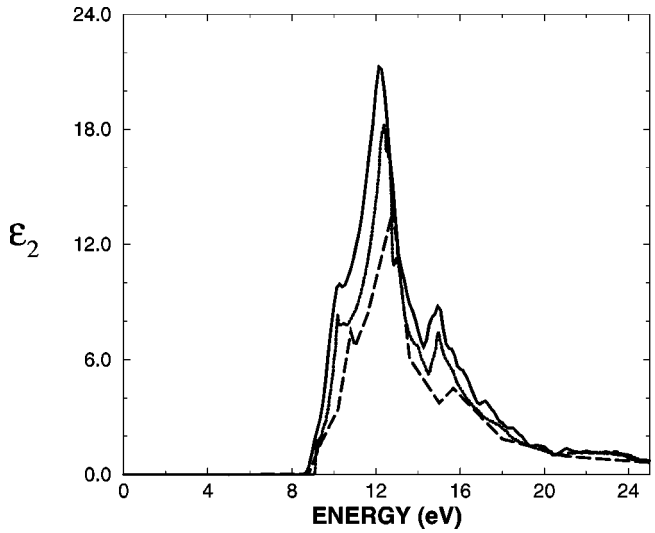

FIG. 5. Calculated imaginary part of dielectric function of c-BN (solid line) vs LMTO result after Ref. 74 (dotted line) and LCAO result (dashed line) of Ref. 25.

crystalline (a) and a microcrystalline (b) sample. Both the spectra show peaks at 11.7 and 1.0 eV and a broad structure around 18 eV. The authors of Ref. 47 claim that the first two peaks correspond to the $E1$ and $E2$ peaks of the zinc-blende-type semiconductors.[73] Our theoretical curve shows two structures centered at 10 eV and 12.7 eV but no clear evidence of higher-energy peaks.

In Fig. 4 we report the calculated dielectric function for *c*-BN obtained within DFT-LDA. The static dielectric constant is found to be 5.45, larger than the experimental one (4.45).[73] This fact must be ascribed to absence of local field effects in the calculation of ϵ_2.[36,60] Experimental curves obtained from recent optical reflectance measurements in the energy range 5–25 eV with syncrotron radiation by Osaka and co-workers[47] are also reported. They used two different samples, namely a sintered *c*-BN plate (short-dashed curve in Fig. 4) and a *c*-BN thin film (long-dashed). The *c*-BN sintered plate produced at high pressure and temperature, offered by Sumimoto Electric Industry (Japan), had dimensions of $5\times5\times0.5$ mm^3 and was characterized as cubic by using x-ray diffraction and Raman scattering.[47] The film, on the other hand, was grown using chemical vapor deposition (CVD) on a silicon substrate, with negative self-bias. The *c*-BN phase, synthesized from B_2H_6 (Ar dilution) and N_2 gas mixtures, had 100–200 Å grain size, confirmed by transmission electron microscopy images.

In Fig. 5 we also compare our curve with that calculated by Xu and Ching,[25] and with a linear muffin-tin orbital (LMTO) one calculated at our theoretical lattice parameter.[74] It is significant to discuss this figure in detail. The experimental data show major structures *A* and *B* at 9.05 and 11.7 eV and shoulders at 13.2 and 16.7 eV (*C* and *D*) for the crystalline sample. In the ϵ_2 in the *c*-BN film, the peak *A* and the shoulders *C* and *D* are not present. The spectrum of the *c*-BN thin film deposited by plasma CVD is similar to that of *c*-BN synthesized under high pressure and high temperature. The authors of Ref. 47 claim that the differences between their spectra are a demonstration of the fact that microcrystalline *c*-BN does not grow epitaxially on a silicon substrate, and presents a rough surface. They do not mention the value of the absorption onset, but a value of 6.8 eV can be deduced from their figure of ϵ_2. To consider the correspondence with the electronic transitions, peak *A* has been associated with the transition Γ_{15v}-Γ_{15c}, peak *B* with the transitions X_{5v}-X_{3c} and X_{5v}-X_{1c}, peak *C* with the transition L_{3v}-L_{3c}, and peak *D* at 16.7 eV with L_{1v}-L_{1c}.[47] The present DFT-LDA reflectance spectrum reproduces the experimental curves qualitatively, but the first peak is found at 12.8 eV and the next at 15.2 eV. Figure 5 also demonstrates that our results do agree with other theoretical calculations (moreover, the theoretical curves show no remarkable difference in the range 25–40 eV which has not been shown in this figure). However, the absorption onset obtained within DFT-LDA is at 8.9 eV, i.e., much higher than the experimental one. This issue turns out to be rather singular in view of the fact that usually, due to the above mentioned band gap problem, the DFT-LDA calculated absorption onset should fall at lower energies than the experimental one.[35,36,25,62] In our case the LDA theoretical curve is blueshifted by more than 2 eV with respect to the experiment. A similar overestimate is found also in other theoretical calculations.[25,36,35] The interpretation of Christensen and Gorczyca[35] for ϵ_2 is different (away from threshold) from that proposed by Osaka and co-workers[47] and by Xu and Ching,[25] and from our interpretation. In fact the authors of Ref. 35 associate the *A* peak with the transitions 3–5 at the $\frac{1}{2}\Gamma$-U point, the major peak *B* with the 4-5 transitions at the Σ and L points, the *C* peak with the 4-6 transitions at L, and the *D* peak with the transition 4-6 at Δ and at Σ'. The onset is ascribed to direct transition at Γ. Xu and Ching found *A*, *B*, and *D* structures, respectively, at 10.7, 12.6, and 15.6 eV, but no evidence for the *C* shoulder in their results.[25] Also, their data show a rigid blueshift with respect to the experimental curve by about 1.7 eV. Our results resemble those of Xu and Ching. Please note that their name assignments for the spectrum do not match the present ones. Our

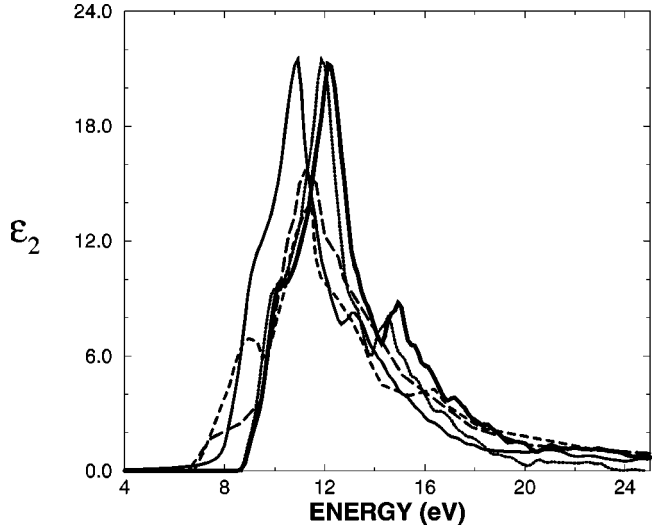

FIG. 6. Calculated imaginary part of dielectric function of *c*-BN at experimental (dotted line), theoretical (bold solid line), and theoretical plus 5% (solid line) lattice constants. Experimental results (dashed lines) after Ref. 47 are plotted for reference.

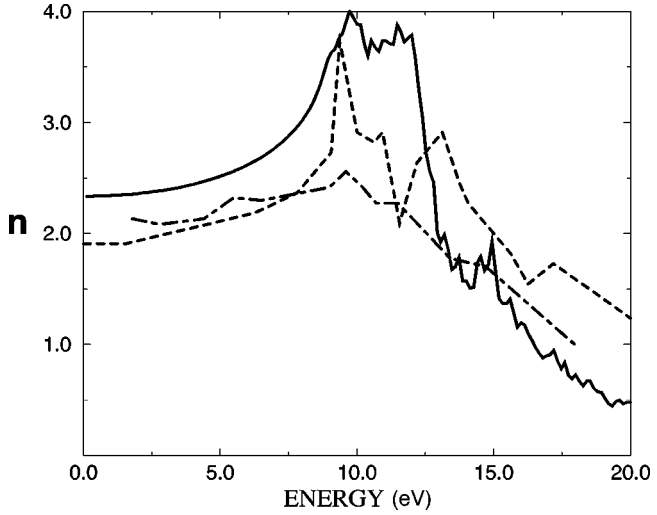

FIG. 7. Calculated real part of refractive index of *c*-BN (solid line) vs the experimental results (dot-dashed line after Ref. 46) , and previous theoretical result (dashed line after Ref. 25).

onset is found at 9.05 eV, while the structures *A*, *B*, and *C* are found respectively at 9.7, 12.5, and 14.9 eV, with small evidence of peak *D*. Our assignment to band transitions within DFT-LDA agrees with that proposed in Ref. 47, and has also been confirmed by Tsay and co-workers.[27]

As far as we know the only other existing experimental data for the minimal direct gap of *c*-BN are those of Philipp and Taft,[3] which yield a value of 14.5 eV. They studied diamond in the vacuum ultraviolet, and they reported data for a *c*-BN sample displaying structures around 9 and 10 eV, and a peak near 14.5 eV.[3] The BN data were reported as marginal by the authors, to support the evidence for a larger direct band gap in *c*-BN than in diamond. Their value of 14.5 eV has been considered as the experimental direct band gap of this material by other authors.[33,73] On the other hand, these data could be interpreted in good agreement with our DFT-LDA spectra. In fact, one could consider the first structure as the display of the onset (at 9 eV in our DFT-LDA calculation) and the major peak as the maximum (at 12.5 eV in our DFT-LDA calculation) (see Figs. (2–4)).

Let us now address in detail the main mismatch between theoretical results (including ours) and the experiments, concerning the onset. One of the points to be considered is the problem of the correct value of the lattice parameter to be used in optical property calculations. This issue has been raised for BN in experimental and theoretical work.[47,36] In Fig. 6 we report different DFT-LDA curves for ϵ_2 calculated at different lattice parameters around the equilibrium one. It is evident that the onset of the theoretical absorption agrees with the experimental one only when the lattice constant is expanded, with respect to the equilibrium one, by 5%. This value appears to be too large, both with respect to the experimental one, and in view of the facts that usually the DFT-LDA underestimation of the lattice constant is about 1%,[75,76] and usually the DFT-LDA underestimates the absorption onset. Another possibility is that the sample under experimental study has not been carefully characterized, namely, concerning different possibilities of disturbances, such as thermal ones, or the presence of (oxide) overlayers,[36,47] which we will not address here but which cannot be excluded in principle. In the following, we consider instead the possibility of *h*-BN contamination within the *c*-BN sample. This is possible due to the fact that in normal conditions *h*-BN domains may be found in *c*-BN samples.[77]

In Fig. 7 and Fig. 8 we also report the real and imaginary parts of the refractive index $n(\omega)$ in comparison with the experimental data of Miyata and co-workers.[46] The experimental data were obtained from reflectance measurements over a photon energy range between 2 and 23 eV, and from transmittance data in the range 2–7 eV. A single crystal of *c*-BN (5 mm^2 area $\times 0.16$ mm thick) was used. Both the onset of the absorption and the imaginary part of the refractive index indicate a gap of 6.1 ± 0.5 eV. Our results are only

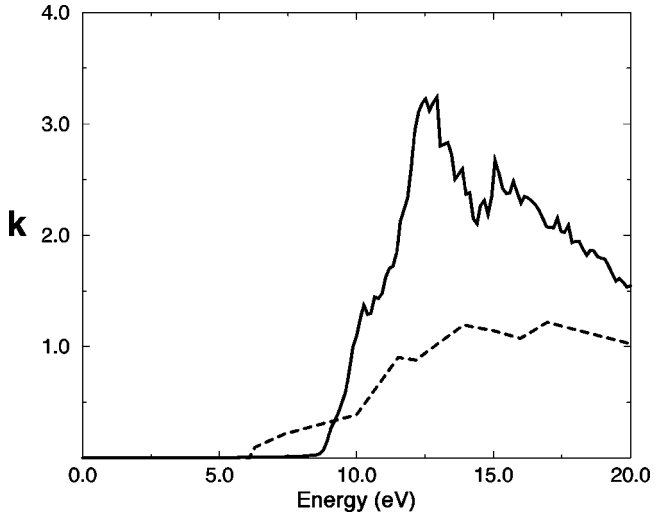

FIG. 8. Calculated imaginary part of refractive index of *c*-BN (solid line) vs experimental results (dashed line) after Ref. 46.

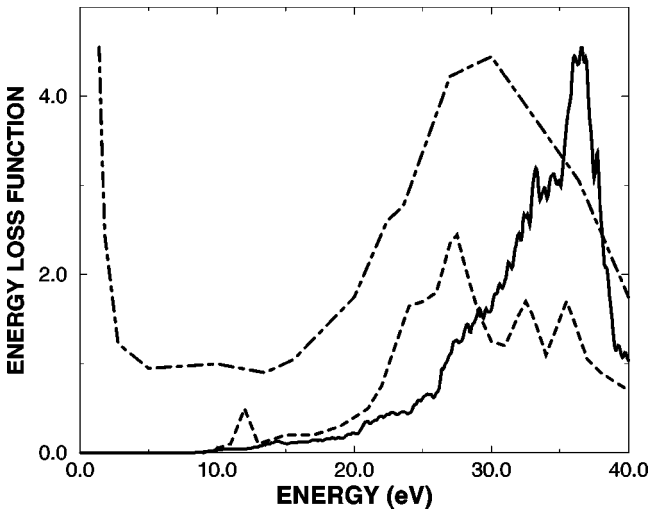

FIG. 9. Energy-loss function of *c*-BN (solid line) vs the experimental result (dot-dashed line) after Ref. 43 and previous theoretical result (dashed line) of Ref. 25.

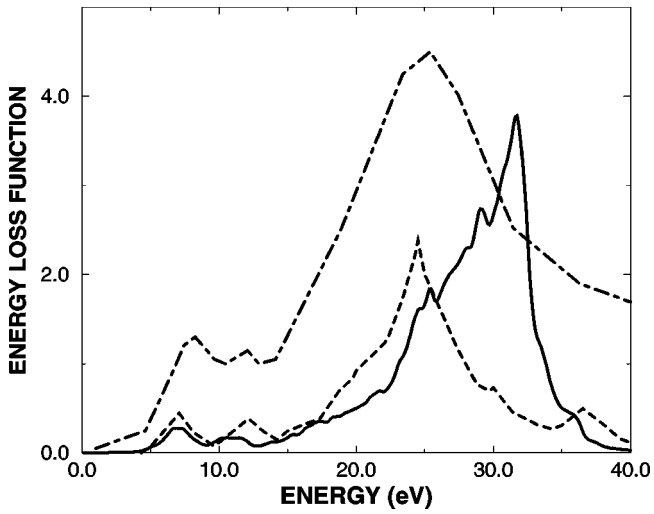

FIG. 10. Energy-loss function of *h*-BN (solid line) vs the experimental result (dot-dashed line) of Ref. 43 and previous theoretical result (dashed line) after Ref. 25.

in qualitative agreement with these measurements.

We can argue that part of the error comes from the normalization imposed on the experimental curves. In fact, the absolute values of reflectance and transmittance were obtained by the authors of Ref. 46 by requiring that the refractive index at $\omega=2.10$ eV is equal to 2.117, the value determined in an independent experiment in Gielisse.[78] Within the present work, instead, no adjustable parameter has been used to fit the experimental data.

In Fig. 9 we report the calculated DFT-LDA energy-loss function for cubic BN, namely, $\mathrm{Im}[-1/\epsilon(q,\omega)]$, in comparison with the experiments. We compare our results with electron energy-loss (EEL) measurements of McKenzie *et al.*[43] The dominant maximum in the EEL spectrum is due to the plasmon excitation, a longitudinal oscillation of the valence electrons as a whole against the cores, classically occurring at frequency $\omega_p^2=Ne^2/m$ where N represents the densities of the valence electrons of the sample. Due to the different density of *h*-BN and *c*-BN, EEL spectra have been used to discriminate between the two phases within the same specimen.[43] The measured ω_p for *h*-BN is 25.5 eV and for *c*-BN it is 28.5 eV. An absorption threshold for the cubic phase at 9 eV was deduced by the authors of Ref. 43. Our DFT-LDA calculation yields a first peak at 33.3 eV, which is in reasonable agreement with the experimental one (28.5 eV) and with that determined by Xu and Ching (28 eV).[25]

V. LAYERED HEXAGONAL BN

For this material conflicting experimental and theoretical values of the fundamental band gap can be found in the literature. Tarrio and Schnatterly presented EEL spectra between 0 and 60 eV, with a plasmon peak at 26.4 eV. From their data, a direct gap of 5.9 ± 0.2 eV was inferred.[45] Catellani and co-workers using a full-potential linear augmented plane wave computational scheme (FLAPW-LDA), claimed that *h*-BN has a minimal indirect gap at the H_{3v}-M_{1c} transition, corresponding to 3.9 eV, and a minimal direct gap at 4.3 eV, corresponding to the H_{3v}-H_{2c} transition.[31] Hoffman and co-workers, by optical reflectivity measurements in the range 0.045–10 eV, found a direct gap of 5.2 ± 0.2 eV, deducing that it corresponded to direct transitions at H.[48] Park, Terakura, and Hamada, using a FLAPW (LDA) scheme, found a minimal direct gap, and gave for the M_v-M_c transition energy a value of 4.5 eV.[30] Last but not least, the work of Suhr and co-workers[33] and of Cappellini *et al.* found, within DFT-*GW*, that the material has an indirect minimal gap (see Sec. III). For *h*-BN we start the discussion with the EEL function reported in Fig. 10. In this figure, we compare the calculated DFT-LDA curve, averaged over the three crystallographic axes, with the curve calculated by Xu and Ching,[25] and with the experimental one by McKenzie *et al.*[43] We recognize three major structures. In the theoretical spectrum of Ref. 25, a first peak (*A*) around 7 eV can be found, a second peak (*B*) is at 12 eV, and a major structure (*C*) appears at 24 eV. The last is the bulk plasmon peak, to be compared with the experimental value of 25.5 eV.[43] In Fig. 11 we report the calculated imaginary part of the dielectric function for averaged *x*-*y* and *z* components. Our results compare well also in this case with the LCAO values by Xu and Ching. In Fig. 12 we plot the imaginary part of the dielectric function averaged over the three crystallographic axes. In particular, from Fig. 11 and Fig. 12, we agree with the conclusions of Xu and Ching that peak *B* in the EEL function of Fig. 10 comes from the component of ϵ_2 parallel to the *c* axis of the hexagonal crystal, while peak *A* comes from the perpendicular components of ϵ_2. These statements may be easily confirmed by considering experimental curves at different scattering momentum transfer (in-plane versus *c*-axis data).[25,45] The major peak *C* contains contributions from both the ϵ_2 components perpendicular and parallel to the *c* axis. In Fig. 13 we report the imaginary and real parts of the calculated refractive index. Again, a qualitative difference to respect with the cubic case is observable. In fact, although the imaginary part of the dielectric function has been averaged over the three crystallographic directions,

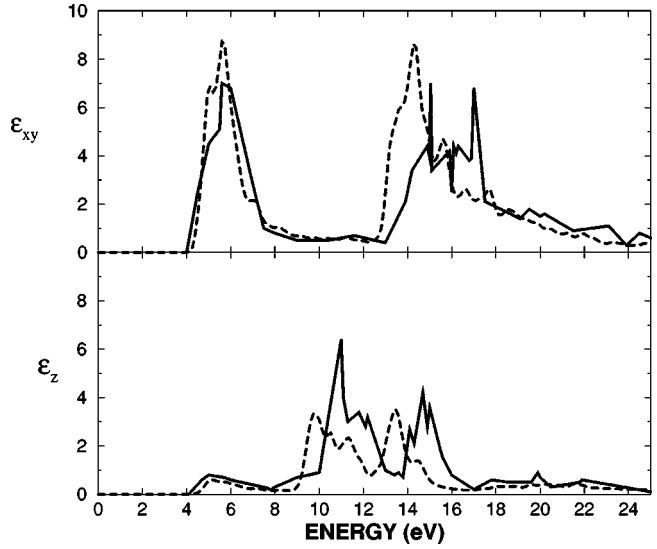

FIG. 11. Top panel: imaginary part of the dielectric function of *h*-BN (solid line) averaged for *x* and *y* directions vs the same quantity after Ref. 25 (dashed line). Bottom panel: imaginary part of the dielectric function of *h*-BN (solid line) in the *z* direction vs the same quantity after Ref. 25 (dashed line).

large differences arise with respect to the cubic case [see Fig. (8)].

A knowledge of the optical properties of *h*-BN can help us to understand the mismatch between theory and experiments for the ϵ_2 of *c*-BN. In fact, as was recently shown,[77] *c*-BN films may display a hexagonal-like top layer, and in the presence of disturbances the amount of disorder in both types of film increases significantly, leading to the transformation of the cubic phase to the hexagonal-like material. Moreover, it has been demonstrated that, due to the large hysteresis of the hexagonal-cubic phase transition, *h*-BN domains may continue to exist in *c*-BN samples.[15] It can hence

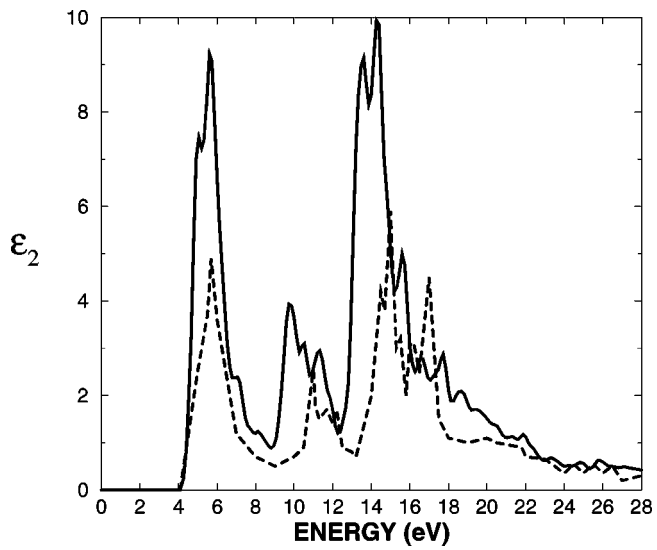

FIG. 12. Imaginary part of dielectric function of *h*-BN (solid line) vs previous theoretical result of Ref. 25 (dashed line) averaged over the three crystallographic directions.

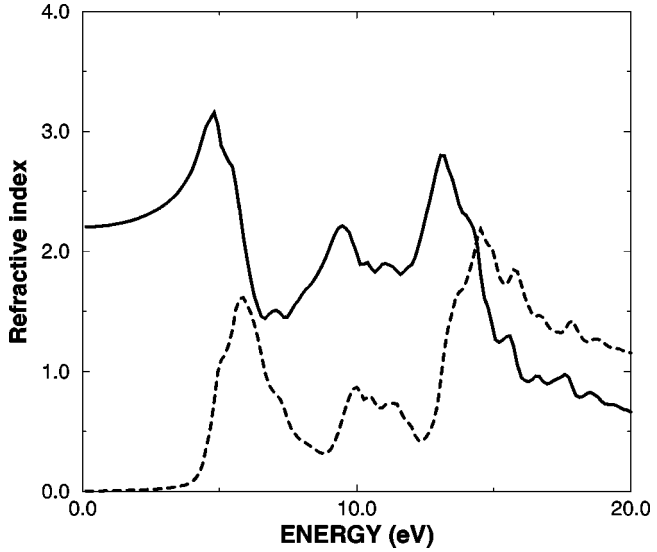

FIG. 13. Calculated refractive index of *h*-BN: real (solid line) and imaginary (dotted line) parts.

be argued that the experimental samples of *c*-BN are likely to contain impurities due to *h*-BN domains. Assuming that the sample used in the experimental work by Osaka and co-workers[47] contained *h*-BN domains, we can work within the effective crystal approximation, i.e., assuming that the domains are homogeneous and isotropic. In this case an imaginary dielectric function corresponding to a linear combination of the two pure forms can be expected for the merged system:[79]

$$\epsilon_2(\omega) = x\,\epsilon_2^{h\text{-BN}}(\omega) + (1-x)\,\epsilon_2^{c\text{-BN}}(\omega) \qquad (4)$$

with *x* going from 0 to 0.5. In Fig. 14 we report the results obtained within this scheme at the DFT-LDA level. By increasing the concentration of the *h* phase, a peak at 5 eV due

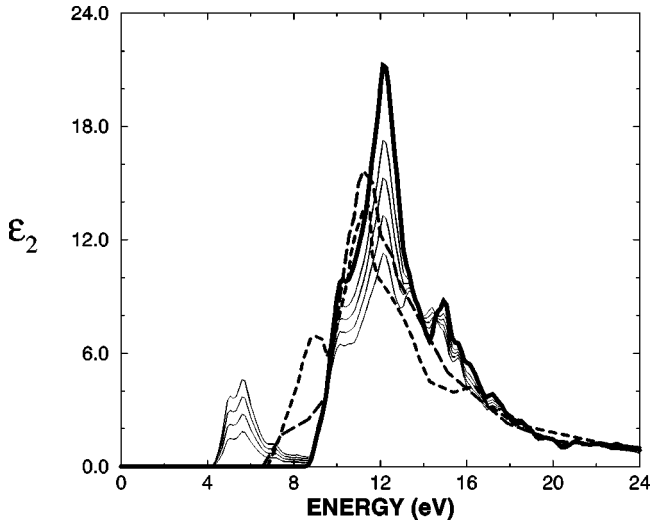

FIG. 14. Imaginary part of dielectric function for merged *c*-BN and *h*-BN (solid lines). The experimental results of Ref. 47 are also given (dashed lines). Pure cubic ϵ_2 is showed with the bold solid line.

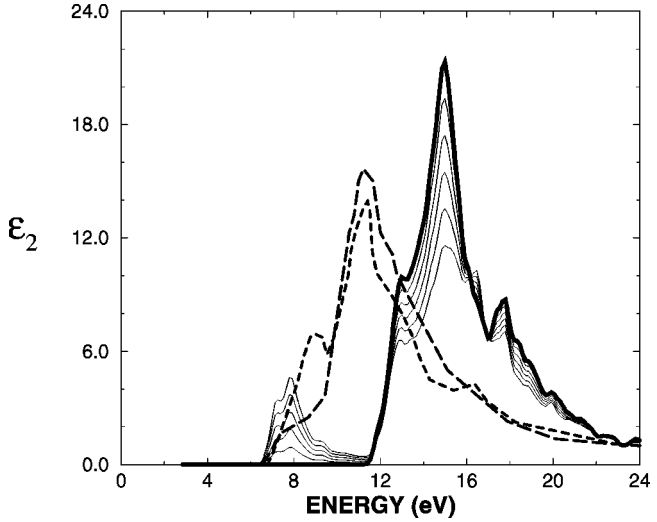

FIG. 15. Imaginary part of dielectric function with *GW* corrections (see text) for merged *c*-BN and *h*-BN (solid lines). Experimental results of Ref. 47 are also given (dashed lines). Pure cubic ϵ_2 is showed with the bold solid line.

to *h*-BN does grow, while the peak around 12 eV due to the cubic phase decreases. Even though the main peak comes into better agreement with the experiments in intensity, the peak around 5 eV remains significantly redshifted with respect to the experimental onset. To address this issue more deeply, we calculated self-energy corrections to the spectra of both phases within the *GW* approximation.[17] The results are reported in Fig. 15. The *GW* corrected spectrum matches the experimental threshold better than the DFT-LDA one, but the major peak now completely misses the main experimental structure at 11.7 eV.

Another possible explanation for the mismatch between theory and experiment for the cubic phase is the contribution of higher-order effects in the spectra, like those due to the electron-hole interaction which we have neglected so far. If we consider, in Fig. 15, the case with $x=0$ (pure *c*-BN with *GW* self-energy corrections), the *GW* theoretical onset falls at 11.6 eV (see Sec. I), more than 5 eV higher than the experimental one ($\sim$5.8 eV from Ref. 47). Hence the inclusion of self-energy effects in the DFT-LDA spectrum worsens the comparison with experiments in the present case. An effect of this type is typical for systems where the excitonic effects are large. The excitonic binding energies, in fact, can range from a few meV (as in bulk GaAs and Si) to much larger values (of the order of 1 eV) in insulating oxides.[80–82] The effects of self-energy and excitonic corrections to the DFT-LDA ϵ_2 curve roughly correspond to shifts in opposite directions.[80,82] Referring to the onset of ϵ_2, one might obtain a rough estimate of the excitonic binding energy from the mismatch between the *GW* corrected onset and the experimental one. In the *c*-BN case, a value of more than 5 eV would result. This value seems to be too high, even in comparison with the strongest exciton binding energies found in systems like oxides, where, due to weak screening, the electron and hole can be bound by an energy of the order of 1 eV.[80] A theoretical evaluation based on Wannier functions for *c*-BN leads to a value of this order of magnitude.[83] To fully address this problem from the theoretical point of view, one should solve the Bethe-Salpeter equation for the optical response function including two-particle effects.[80–82] One should also look for more refined experimental measurements of the linear optical properties of *c*-BN. In summary, *c*-BN and *h*-BN mixing within the sample, self-energy and excitonic effects, the presence of impurities, the lack of pure crystalline samples, and lattice parameter mismatch, can in principle all be sources of the disagreement between theoretical results and the available spectra for *c*-BN.

VI. CONCLUSIONS

Linear optical functions of cubic and hexagonal BN have been studied within DFT-LDA. Calculated energy-loss functions compare reasonably well with experiments and with previous theoretical results, for both *h*-BN and *c*-BN. Discrepancies arise between theoretical results and experiments in the imaginary part of the dielectric function for *c*-BN. Possible explanations of this issue are proposed and evaluated: lattice constant variations, *h*-BN contamination in *c*-BN samples, and self-energy effects. On the other hand, our DFT-LDA results show a reasonable agreement with other theoretical outcomes and with experiments for the imaginary part of the dielectric function in the case of *h*-BN. More refined measurements and calculations are needed to fully address the mismatch between theory and experiment for the cubic case. In future work we intend to go further in the direction of a refinement of the calculations.

ACKNOWLEDGMENTS

We thank R. Del Sole, P. Monachesi, G. Adragna, and A. Marini for useful discussions. We acknowledge the help of G. Pusceddu in generating pseudopotentials used in this work.

[1] L. Kleinmann and J. C. Phillips, Phys. Rev. **117**, 460 (1960).
[2] E. Doni and G. Pastori Parravicini, Nuovo Cimento B **64**, 117 (1969).
[3] H. R. Philipp and E. A. Taft, Phys. Rev. **127**, 159 (1962).
[4] J. H. Edgar, in *Properties of Group III Nitrides*, edited by J. H. Edgar (Institution of Electric Engineers, Stevenage, UK, 1994), pp. 7–21.
[5] T. K. Pauli, P. Bhattacharya, and D. N. Bose, Appl. Phys. Lett. **56**, 2648 (1990).
[6] S. S. Dana, Mater. Sci. Forum **54-55**, 229 (1990).
[7] K. Miyoshi, D. H. Bukley, J. J. Pouch, S. A. Alterovitz, and H. E. Sliney, Surf. Coat. Technol. **33**, 221 (1987).
[8] X. Blase, A. Rubio, S. G. Louie, and M. L. Cohen, Europhys. Lett. B **28**, 335 (1994).

[9] A. Rubio, J. L. Corkill, and M. L. Cohen, Phys. Rev. B **49**, 5081 (1994).
[10] X. Blase, A. Rubio, S. G. Louie, and M. L. Cohen, Phys. Rev. B **51**, 6868 (1995).
[11] L. Vel, G. Demazeau, J. Etourneau, and J. J. Pouch, Mater. Sci. Eng., B **10**, 149 (1991).
[12] M. J. Powers, M. C. Benjamin, L. M. Porter, R. J. Nemanich, R. F. Davis, J. J. Cuomo, G. L. Doll, and S. J. Harris, Appl. Phys. Lett. **65**, 3912 (1995).
[13] R. W. Pryor, Appl. Phys. Lett. **68**, 13 (1996).
[14] B. F. Williams and R. E. Simon, Appl. Phys. Lett. **14**, 214 (1969).
[15] M. I. Eremets, K. Takemura, H. Yusa, D. Goldberg, Y. Bando, V. D. Blank, Y. Sato, and K. Watanabe, Phys. Rev. B **57**, 5655 (1998).
[16] V. L. Solozhenko, J. Hard Mater. **6**, 51 (1995).
[17] G. Cappellini, V. Fiorentini, K. Tenelsen, and F. Bechstedt, in *Gallium Nitride and Related Materials*, edited by R. D. Dupuis, J. A. Edmond, F. A. Ponce, and S. Nakamura, Mater. Res. Soc. Symp. Proc. No. **395** (Materials Research Society, Pittsburgh, 1996), p. 429.
[18] V. L. Solozhenko, in *Properties of Group III Nitrides* (Ref. 4).
[19] G. Kern, G. Kresse, and J. Hafner, Phys. Rev. B **59**, 8551 (1999).
[20] M. Sokolowski, J. Cryst. Growth **46**, 136 (1979).
[21] J. Furthmüller, J. Hefner, and G. Kresse, Phys. Rev. B **50**, 15 606 (1994).
[22] K. Albe, Phys. Rev. B **55**, 6203 (1997).
[23] R. M. Wentzcovitch, K. J. Chang, and M. L. Cohen, Phys. Rev. B **34**, 1071 (1986).
[24] R. M. Wentzcovitch, S. Fahy, M. L. Cohen, and S. G. Louie, Phys. Rev. B **38**, 6191 (1988).
[25] Y.-N. Xu, W. Y. Ching , Phys. Rev. B **44**, 7787 (1991).
[26] A. Zunger, A. Katzir, A. Halperin, Phys. Rev. B **13**, 5560 (1976).
[27] Y. F. Tsay, A. Vaidyanathan, and S. S. Mitra, Phys. Rev. B **19**, 5422 (1979).
[28] R. Dovesi, C. Pisani, C. Roetti, and P. Dellarole, Phys. Rev. B **24**, 4170 (1981).
[29] J. Robertson, Phys. Rev. B **29**, 2131 (1984).
[30] K. T. Park, K. Terakura, and N. Hamada, J. Phys. C **20**, 1241 (1987).
[31] A. Catellani, M. Posternak, A. Baldereschi, and A. J. Freeman, Phys. Rev. B **36**, 6105 (1987).
[32] P. E. Van Camp, V. E. Van Doren, and J. T. Devreese, Solid State Commun. **71**, 1055 (1989).
[33] M. P. Suhr, S. G. Louie, and M. L. Cohen, Phys. Rev. B **43**, 9126 (1991).
[34] Y.-N. Xu and W. Y. Ching, Phys. Rev. B **48**, 4335 (1993).
[35] N. E. Christensen and I. Gorczyca, Phys. Rev. B **50**, 4397 (1994).
[36] V. I. Gavrilenko and R. Q. Wu, Phys. Rev. B **61**, 2632 (2000).
[37] G. Cappellini, G. Satta, K. Tenelsen, and F. Bechstedt, Phys. Status Solidi B **95**, 861 (2000).
[38] R. D. Carson and S. E. Schnatterly, Phys. Rev. Lett. **59**, 319 (1987).
[39] J. J. Jia, T. A. Callcot, E. L. Shirley, J. A. Carlisle, L. J. Terminello, A. Asfaw, D. L. Ederer, F. J. Himpsel, and R. C. C. Perera, Phys. Rev. Lett. **76**, 4054 (1996).
[40] C. Oshima and A. Nagashima, J. Phys.: Condens. Matter **9**, 1 (1997).
[41] B. M. Davies, F. Bassani, and F. C. Brown, Phys. Rev. B **24**, 3537 (1981).
[42] I. Jimènez, A. F. Jankowski, L. J. Terminello, J. A. Carlisle, D. G. J. Sutherland, G. L. Doll, J. V. Mantese, W. M. Tong, D. K. Shuh, and F. J. Himpsel, Phys. Rev. B **55**, 12 025 (1997).
[43] D. R. McKenzie, W. G. Sainty, and D. Green, Mater. Sci. Forum **54-55**, 193 (1990).
[44] U. Büchner, Phys. Status Solidi B **81**, 227 (1977).
[45] C. Tarrio and S. E. Schnatterly, Phys. Rev. B **40**, 7852 (1989).
[46] N. Miyata, K. Moriki, O. Mishima, M. Fujisawa, and T. Hattori, Phys. Rev. B **40**, 12 028 (1989).
[47] Y. Osaka, A. Chayahara, H. Yokohama, M. Okamoto, T. Hamada, T. Imura, and M. Fujisawa, in *Synthesis and Properties of Boron Nitride*, edited by J. J. Pouch and S. A. Alteroviz , Vols. 54 & 55 (Trans Tech, Aedermannsdorf, Switzerland, 1990), pp. 277–294.
[48] D. M. Hoffman, G. L. Doll, and P. C. Eklund, Phys. Rev. B **30**, 6051 (1984).
[49] R. M. Chrenko, Solid State Commun. **14**, 511 (1974).
[50] R. M. Dreizel and E. K. U. Gross, *Density Functional Theory* (Springer, New York, 1990).
[51] J. P. Perdew and A. Zunger, Phys. Rev. B **23**, 5048 (1981).
[52] D. M. Ceperley and B. J. Alder, Phys. Rev. Lett. **45**, 566 (1980).
[53] X. Gonze, R. Stumpf, and M. Scheffler, Phys. Rev. B **44**, 8503 (1991).
[54] M. Fuchs and M. Scheffler, Comput. Phys. Commun. **119**, 67 (1999).
[55] N. Troullier and J. L. Martins, Phys. Rev. B **43**, 1993 (1991).
[56] S. G. Louie, S. Froyen, and M. L. Cohen, Phys. Rev. B **26**, 1738 (1982).
[57] D. J. Chadi and M. L. Cohen, Phys. Rev. B **8**, 5747 (1973).
[58] C. R. Aita, in *Synthesis and Properties of Boron Nitride* (Ref. 47), pp. 1–20.
[59] O. Pulci, G. Onida, A. I. Shkrebtii, R. Del Sole, and B. Adolph, Phys. Rev. B **55**, 6685 (1997).
[60] B. Adolph, V. I. Gavrilenko, K. Tenelsen, F. Bechstedt, and R. Del Sole, Phys. Rev. B **53**, 9797 (1996).
[61] F. Bassani and G. Pastori Parravicini, *Electronic States and Optical Tansitions in Solids* (Pergamon Press, Oxford, 1973); A. Baldereschi and A. Quattropani (unpublished).
[62] M. S. Hybertsen and S. G. Louie, Phys. Rev. B **34**, 5390 (1986).
[63] F. Bechstedt, Festkoerperprobleme **32**, 161 (1992).
[64] F. Bechstedt and R. Del Sole, Phys. Rev. B **38**, 7710 (1988).
[65] F. Gygi and A. Baldereschi, Phys. Rev. Lett. **62**, 2160 (1989).
[66] L. Hedin, Phys. Rev. **139**, A796 (1965); L. Hedin and S. Lundqvist, Solid State Phys. **23**, 1 (1969).
[67] R. Godby, M. Schlüter, and L. J. Sham, Phys. Rev. B **37**, 10 159 (1988).
[68] F. Bechstedt, R. Del Sole, G. Cappellini, and L. Reining, Solid State Commun. **84**, 765 (1992).
[69] M. Palummo, R. Del Sole, Lucia Reining, F. Bechstedt, and G. Cappellini, Solid State Commun. **95**, 393 (1995); B. Wenzien, G. Cappellini, and F. Bechstedt, Phys. Rev. B **51**, 14 701 (1995); B. Wenzien, P. Käckell, F. Bechstedt, and G. Cappellini, *ibid.* **52**, 10 897 (1995).
[70] M. S. Hybertsen and S. G. Louie, Phys. Rev. B **37**, 2733 (1988).
[71] G. Cappellini, S. Bouette-Russo, B. Amadon, C. Noguera, and F. Finocchi, J. Phys.: Condens. Matter **12**, 3671 (2000).
[72] X. Blase, A. Rubio, S. G. Louie, and M. L. Cohen, Phys. Rev. B **51**, 6868 (1995).

[73] O. Madelung, *Semiconductor Basic Data* (Springer, Berlin, 1996).
[74] P. Monachesi (private communication).
[75] M. Palummo, L. Reining, R. W. Godby, C. M. Bertoni, and N. Borsen, Europhys. Lett. **26**, 607 (1994).
[76] V. Fiorentini, Phys. Rev. B **46**, 2086 (1992).
[77] P. Widmayer, H.-G. Boyen, P. Ziemann, P. Reinke, and P. Oelhafen, Phys. Rev. B **59**, 5233 (1999).
[78] P. J. Gielisser, S. S. Mitra, J. M. Plendl, R. D. Griffis, L. C. Manasur, R. Marshall, and E. A. Pascoe, Phys. Rev. **155**, 1039 (1967).
[79] V. Fiorentini and A. Baldereschi, J. Phys.: Condens. Matter **4**, 5967 (1992), and references therein.
[80] S. Albrecht, G. Onida, and L. Reining, Phys. Rev. B **55**, 10 278 (1997).
[81] S. Albrecht, L. Reining, R. Del Sole, and G. Onida, Phys. Status Solidi A **170**, 189 (1998).
[82] M. Rohlfing and S. G. Louie, Phys. Rev. Lett. **81**, 2312 (1998).
[83] G. Adragna, MS thesis, II University of Rome, 1998 (private communication).